

# Diesel spray formation, autoignition and soot production at elevated in-cylinder pressures

by

C. Crua<sup>(1)</sup> and M.R. Heikal<sup>(2)</sup>

Internal Combustion Engine Group, School of Engineering,  
University of Brighton, Brighton BN2 4GJ, UK

<sup>(1)</sup>E-Mail: [C.Crua@brighton.ac.uk](mailto:C.Crua@brighton.ac.uk)

<sup>(2)</sup>E-Mail: [M.R.Heikal@brighton.ac.uk](mailto:M.R.Heikal@brighton.ac.uk)

M.R. Gold

Ricardo Consulting Engineers

Bridge Works, Shoreham-by-Sea BN43 5FG, UK

E-Mail: [Martin.Gold@ricardo.com](mailto:Martin.Gold@ricardo.com)

## ABSTRACT

Through the combination of various optical diagnostic techniques an analysis has been undertaken of the effects of in-cylinder and injection pressures on the formation and combustion of diesel sprays at realistic automotive in-cylinder conditions. The results were obtained with high-speed video and phase Doppler anemometry (PDA) of the liquid phase, high-speed schlieren video of the vapour phase, high-speed video of autoignition and laser-induced incandescence (LII) of soot. Output results containing spray dispersion angles, droplet sizes and velocities, tip penetrations with time, autoignition delays and relative soot concentrations are presented offering an insight into the common rail diesel spray formation, mixing and combustion processes.

The tests were performed on a single-cylinder 2.2 litre rapid compression diesel machine with optical access to the combustion chamber. A common rail injection system was used with an injector mounted with a single-hole nozzle. The injection pressure was varied from 60 to 160 MPa, the in-cylinder pressure and temperature at top dead centre from 2 to 10 MPa and from 540 to 720 K, respectively.

The results obtained from the various optical measurement techniques were combined in order to produce a comprehensive observation of diesel spray development and combustion.

## 1. INTRODUCTION

The work presented here was undertaken at the University of Brighton, jointly with Ricardo Consulting Engineers, on a new compression machine based on a two-stroke diesel engine modified to allow visualisation of in-cylinder combustion processes (Crua, 2002). This research facility was specifically designed to enable the study of diesel sprays at realistic automotive in-cylinder conditions while simultaneously providing good optical access for both qualitative and quantitative measurements of both combusting and non-combusting sprays. The rig is constructed around a single cylinder two-stroke diesel engine with a specially designed optical chamber incorporated between the cylinder and head. The experimental work can be broadly divided in two main groups: non-combusting spray characterisation and combustion studies. Studying non-combusting sprays allows the assessment of the location of diesel liquid and vapour. This information, which is crucial for correct analysis of combustion, was obtained by several optical techniques:

- Phase Doppler anemometry
- Shadowgraphy, using a backlit high-speed digital video camera.
- Shadowgraphy, using a high-speed spark light flashgun and a 35 mm SLR camera for high-quality imaging of crucial injection phases.
- Schlieren cinematography with a high-speed digital video camera.

Combustion studies were focused on the investigation of the autoignition and soot formation of diesel sprays and has been conducted using the following techniques:

- Flame high-speed cinematography, for assessing the variations of autoignition timing and location.
- In-cylinder pressure measurements, for comparison between combustion pressure rise and flame luminosity data.
- Laser-induced incandescence (LII), for imaging of soot formation sites.

## 2. EXPERIMENTAL APPARATUS

### 2.1. Rapid compression/expansion machine

The spray rig facility was designed specifically to enable the gaps in the current literature (spray and combustion analysis of injections into environments above 6 MPa) to be addressed, in addition to providing a means of testing sprays at conditions anticipated for the next generation of diesel engines. This rapid compression machine is based around a single cylinder Ricardo Proteus test engine which was converted to two-stroke cycle operation by the addition of inlet and exhaust ports in the cylinder liner. This approach significantly increased the room available in the cylinder head for optical access by the removal of inlet and exhaust valves and also allowed reduced mechanical complexity, thus cutting down on engine build times. The engine had a bore of 135 mm, a stroke of 150 mm, and a displacement of 2.2 litres. The cylinder head was heated by a water jacket (90°C) and the sump oil by immersion heaters (85°C). This enabled the engine to be heated prior to motored testing, and therefore minimise heat losses from the compressed gas to the cylinder wall.

A water-cooled Kistler pressure-transducer attached to a storage oscilloscope was used to monitor the in-cylinder pressure. The Proteus was driven by a dynamometer through a 90° gearbox. The output shaft of the gearbox was connected to the Proteus flywheel and, with a reduction ratio of 6:1, reduced the dynamometer speed of 3000 rpm to 500 rpm engine speed. This was the operating engine speed for all the tests carried out in this work. The rail and delivery pipe were both instrumented with Kistler pressure transducers. The pipe from the rail to the injector was kept short, representative of a real vehicle system. The fuel injector used was a modern electro-magnetically actuated common rail injector. This injector was specially equipped with a needle lift sensor to obtain the exact needle position during the injection. The injector nozzles were interchangeable and therefore allowed testing of different nozzle types and nozzle hole diameters. A custom-built controller was developed (Kennaird *et al.*, 2000) to enable independent control of injection timing, number of injections per cycle, injection duration and rail pressure. This unit essentially consisted of a microprocessor dedicated to the task of triggering the injector and a secondary device (such as a laser system, flashgun or CCD camera). The custom controller also allowed control of initial needle drive current and PID control of the fuel rail pressure. Before each series of experiments, a personal computer was used to upload the injection parameters to the FIE unit (e.g. injection angle, injection duration, rail pressure, delay of secondary trigger, etc.). This gave high timing accuracy and good parameter control. For the entire experimental work low-sulphur Esso AF1313 diesel reference fuel was used.

## 2.2. Spray visualisation

The CCD video camera used in this series of experiments was a Kodak Ektapro HS Motion Analyzer (model 4540), with a recording rate adjustable from 30 to 4500 frames per second (fps) at full resolution (256x256 pixels x 256 grey levels), and from 9000 to 40500 fps at progressively reduced resolution. The best compromise between acquisition rate and image resolution was obtained with a frame rate of 18000 to 27000 fps, with a corresponding resolution of 256x64 pixels, and 128x64 pixels, respectively. The sprays were backlit by a halogen flood light fitted with a diffuser.

The processing of the videos was performed by purpose-developed software that measured the spray penetration length and spray cone angle at each video frame after suitable pixel thresholding (Morgan *et al.*, 2001). The images were thresholded to pick out the spray outline from the background. The threshold level was subjectively chosen by selecting one image from the batch of images generated by a test run and varying the threshold to obtain optimum results. Since the quality of images remained the same during a test run, this threshold value was suitable for all the images in that batch. The maximum spray penetration was calculated by finding the spray pixel furthest from the nozzle. The software was used to calculate the spray penetration and dispersion angle for each frame of every video.

## 2.3. PDA instrumentation

The optical experimental set-up, shown in Figure 1, consists of nine components. The light source was a Spectra Physics Argon-ion laser operating in “all lines” modes.

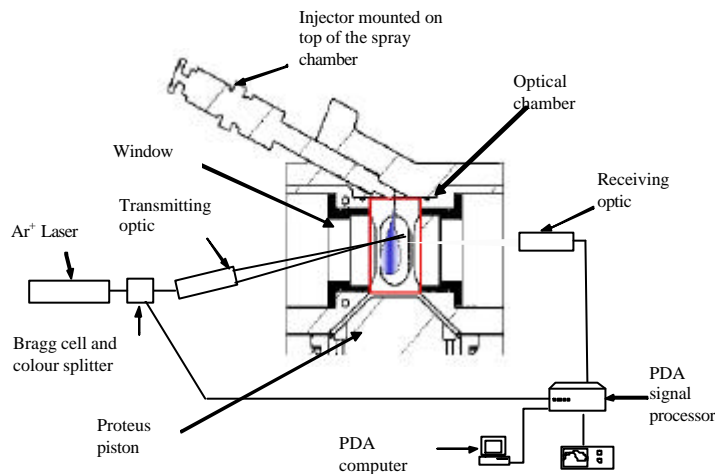


Fig. 1. PDA set-up.

The beam passes through a Bragg cell and colour separator, which splits the incoming beam into two beams and shifts the frequency of one of them. The beams then travel to the transmitting optic through an optical fibre. A lens mounted on the transmitting optic focuses the two beams to form the measurement volume at a focal length of 310 mm. The receiving optic was positioned at 310 mm from the measurement volume, at an angle of 70°. The collection optic consists of a 310 mm focal length lens and four photomultipliers. The lens focuses the scattered light from particles crossing the measurement volume onto four detectors. These convert the fluctuations in light intensity into fluctuations in a voltage signal that could be interpreted by the Doppler signal processor (Dantec BSA P70). The PDA transmitting and receiving optics are mounted on optical rails that are secured onto an air cushioned optical table to avoid ground-transmitted vibrations.

Laser	
Wavelength	514.5 nm
Beam diameter	2.2 mm
Focal length of lenses	
Transmitting optic	310
Receiving optic	310 mm
Beam separation	36 mm
Beam intersection angle	13.116°

Fringe spacing	2.252 $\mu\text{m}$
Number of fringes	20
Probe volume	$9.01 \times 10^{-4} \text{ mm}^3$
Velocity bandwidth	-56.3 to 146.4 m/s
Maximum diameter	45.3 $\mu\text{m}$
Particle refractive index	1.41
Medium refractive index	1.0002
Signal-to-noise ratio level	-3 dB
Sphericity factor	10%

*Table 1. Optical parameters of the PDA system.*

The alignment and focus of the optics were checked periodically with a water spray generated by a pharmaceutical nebuliser. The nebuliser was also used to validate the measurements by generating a cloud of water droplets of a known diameter (3 to 6  $\mu\text{m}$ ) so as to compare them with the obtained PDA data.

#### **2.4. Laser-induced incandescence**

The laser used was a pulsed Nd:YAG laser, capable of delivering pulses of 300 mJ at a frequency of 10 Hz and a wavelength of 532 nm. The laser pulses were spatially and temporally Gaussian with beam diameter of 8.7 mm and pulse width of 6-7 ns at full width at half maximum (FWHM). In order to minimise the effects of window fouling by soot deposit, a fuel additive was used. This additive, Ethyl Hitec 4103 (2-ethylhexyl nitrate,  $\text{C}_8\text{H}_{17}\text{NO}_3$ ), was diluted at the rate of 0.375  $\text{cm}^3$  per litre and raised the fuel cetane number from 55 to 57. The laser sheet had a thickness of 0.75 mm and a height of 55 mm. The measured laser energy output, 290 mJ per pulse, was slightly below the manufacturer's specifications of 300 mJ per pulse. The energy lost through the optical path, i.e. from the laser output to the measurement location, was less than 10 mJ. Hence the laser pulses for LII acquisition had an average energy of 280 mJ each. The intensified CCD camera could acquire monochromatic images of up to  $1280 \times 1024$  pixels with a 12 bit resolution. The resolution of the images presented here was measured to be  $73 \times 73 \mu\text{m}$  per pixel. An image-doubling extension was fitted onto the camera lens to duplicate the view of the combusting spray. Therefore two views of the spray were recorded on one single image, and a different optical filtering could be applied to each half image (Figure 2).

The original intention was to collect simultaneous LII and LIS of soot particles to produce maps of relative soot particle diameter. Although LII was successfully obtained with this configuration, LIS of soot could not be observed. Because the diesel droplets present during the injection scatter much more light than the soot particles, sufficient exposure of the soot scattering could not be obtained without the risk of overloading the photomultiplier tube with droplet scattering. An alternative would have been to gather simultaneous LII / LIS only after the injection had stopped, when no fuel droplets would be expected to be present. Unfortunately, it was observed that this constraint resulted in at least 50% of the soot formation period being discarded. It was also found that interference from LII was not negligible with the LIS filter, resulting in a potentially significant error. Therefore, it was decided that simultaneous LIS of fuel droplets would be recorded to complement the LII of soot.

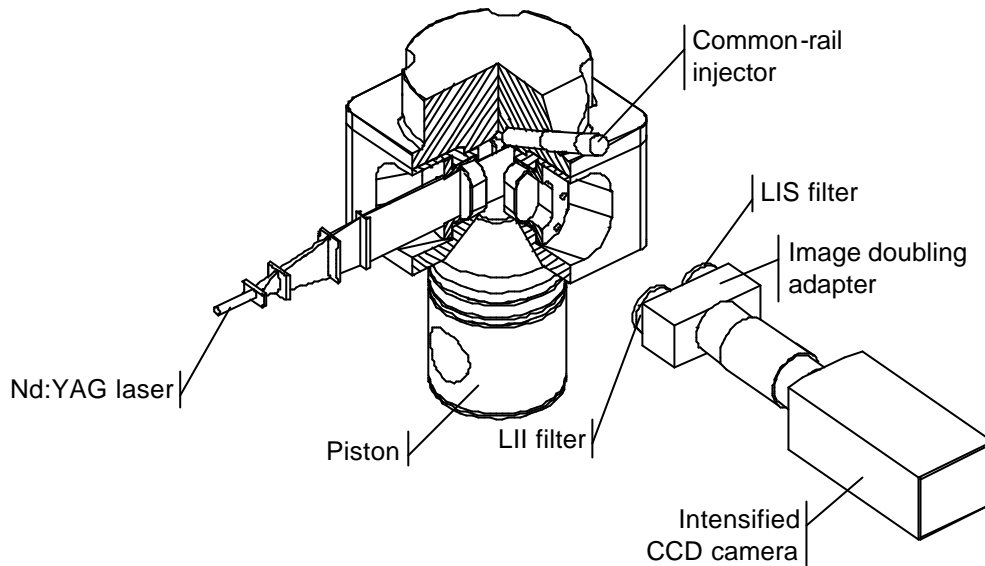


Fig. 2. Experimental set-up for simultaneous LII/LIS study.

This strategy provides information on the location of the liquid fuel spray relative to the soot formation regions. Interference filters were selected to suit the requirements for the study of soot formation. For LII imaging, a wide-bandpass filter was selected, with a measured peak transmission at 416 nm and a 64.4 nm FWHM. This filter maximised the LII signal and offered excellent rejection of interference from elastic scattering, fluorescence and flame luminosity. For LIS imaging, a narrow bandpass filter centred on 532 nm was chosen with a 9.4 nm FWHM. Because the elastic scattering was particularly intense, a set of neutral density filters was used to avoid overloading the photomultiplier tube.

LII images were recorded throughout the soot formation period for three different injection pressures (100, 140 and 160 MPa) and a range of in-cylinder pressures (6, 7, 8 and 9 MPa at non-fired TDC). Because of the turbulent nature of in-cylinder combustion, cycle-to-cycle variations in the position of dense soot regions were expected. This is accentuated by the fact that LII provides a map of soot concentration for a very narrow section of the flame. Therefore, although there may not be significant variations in the flame structure when observed with high-speed video, the positions of dense soot regions may fluctuate greatly within the flame. Hence, consistent information on the characteristics of soot formation cannot be obtained without acquiring a number of images for every combination of engine parameters. Data sets were recorded from the start of soot formation until no soot could be detected, with a time interval between two sets of 0.33 ms (1 CA). Each data set included between 27 and 30 images acquired consecutively during the same run. All images were inspected visually to ensure they were recorded properly and that the repeatability was adequate. The data sets were then post-processed to produce ensemble averaged and standard deviation images for each condition. In order to simplify the presentation and analysis of the data, the mean intensity of each average image was calculated. The mean intensity provides a relative indication of the amount of soot recorded in each data set. The numbers thus obtained were used to produce the LII intensity profiles presented in Section 4. The first step of the processing consisted in obtaining the ensemble averaged and standard deviation images of the data set. The influence of the data set size on the average image was assessed. It was observed that as the size of the data set was progressively increased from 1 to 30 images, the mean intensity of the average image converged rapidly. For data sets of at least 27 images, the coefficient of variation (ratio of standard deviation and mean intensity) was less than 1.7%. Apart from justifying the selected data set size (between 27 and 30 images), this proves the non-random nature of the LII images (convergence was observed).

### 3. ACCURACY OF THE DATA

#### 3.1. High-speed video recordings

Repeatability tests were performed to assess the variability in penetration for a range of test conditions. The variation in spray tip penetration length was found to be  $\pm 4\%$  from the average curve. The camera resolution was measured to be

0.3 mm per pixel, hence the overall uncertainty was estimated to be  $\pm 6\%$ . The calculated results were found to be insensitive to the threshold level chosen with a 12.5% variation in threshold level giving a 1% change in measured penetration (Morgan et al., 2001)

### 3.2. LII data

The LII signal intensity is strongly dependent on laser power density. For a Gaussian beam profile, the LII signal intensity is almost unaffected by variations in laser fluence between 20 and 80 MW cm<sup>-2</sup> (Tait & Greenhalgh, 1993). For this power density range, the error caused by laser fluence fluctuations has an average of 1.9% and a maximum of 3%. This low sensitivity to variations in laser power is believed to be due to the fact that, for a Gaussian beam, an increase in laser energy results in an increase in the effective beam diameter (Zhao & Ladommatos, 1998). Since the laser system used for gathering the LII data had a Gaussian beam with a fluence between 60 and 80 MW cm<sup>-2</sup>, it can be assumed that the results presented here were not significantly affected by shot-to-shot energy fluctuations and longer term fluence drifts. Another advantage of this type of beam lies in the fact that the progressive attenuation of the laser sheet across the dense soot regions of the spray may not result in a strong reduction of the LII signal. This significantly simplifies the post-processing and the interpretation of the LII data, since normalization of the images is not required.

The vaporisation of soot particles induced by the laser results in the production of molecular carbon species (e.g. C<sub>2</sub>, C<sub>3</sub>). C<sub>3</sub>, although believed to be the major vapour constituent, was not observed to produce emissions in LII studies (Wainner, 1999). C<sub>2</sub> is known to produce potentially intense emissions over a broad spectrum, especially at high laser intensities. Since some emission bands of C<sub>2</sub> (438.3, 473.7, 516.5 and 563.6 nm) are well within the preferred LII observation bandwidth, fluorescence from this molecule must be taken into account in order to ensure minimal contamination of the LII signal. Wainner (1999) observed that for a laser fluence below 2 J cm<sup>-2</sup> at 532 nm, the interference from C<sub>2</sub> fluorescence was not significant for collection wavelengths below 440 nm. The characteristics of the laser system used for this study satisfy this condition (laser wavelength = 532 nm; laser fluence < 1.2 J cm<sup>-2</sup>; collection at 416 $\pm$ 32 nm). Wainner (1999) also reported that fluorescence from PAHs, although possibly significant at excitation wavelengths in the UV, was not detected for a laser wavelength of 532 nm. It is therefore concluded that the LII results presented here were not significantly contaminated by fluorescence from PAHs or C<sub>2</sub> molecules.

Ni *et al.* (1995) showed that the LII signal intensity decay was highly dependent on soot particle diameter. They observed that the LII signal could first be detected between 10 and 12 ns after the start of the laser pulse. The rise in signal intensity was reported to last approximately 12 ns and was found to be unaffected by particle size. Following the peak in LII signal intensity, a decay was observed to last up to several hundred nanoseconds. The decay time was shown to be longer for larger soot particles. Ni *et al.* (1995) thus recommended that LII signal should be imaged shortly after the laser pulse, and with reduced exposure times so that size-dependence be minimized. This inherent sensitivity of LII decay time to soot size was used to obtain a measurement of soot primary diameter (Roth & Filippov, 1996; Schraml *et al.*, 1999). The settings used for gathering the LII data presented here follow the recommendations of Ni *et al.* (1995), with an effective LII exposure time of 25 ns. It is estimated that the resulting error caused by size-dependence should be less than 4% (Ni *et al.*, 1995).

Signal trapping is caused by regions of dense soot, located between the laser plane and the CCD camera, and can potentially cause considerable attenuation of the LII signal intensity. Estimation of the extent of signal trapping performed by Wainner (1999) on laminar flames suggest that measured LII signals could be underestimated by as much as 45%. This limitation certainly casts doubt on the validity of any quantitative measurements obtained with the LII technique (including simultaneous LII / LIS of soot) for turbulent flames. However, when used qualitatively, LII images still supply highly valuable information on timing and location of soot formation sites. Potentially, this technique can provide high-resolution data, both temporally and spatially, and has proven invaluable for improving the understanding of combustion processes in diesel engines.

It was observed that the time at which the LII images were recorded was accurate to within 3%. The error caused by contaminations and particle size dependence for the LII data presented here was estimated to be less than 6%. Since this value represents the proportion of spurious emissions within the LII images it can be concluded that it represents the overall measurement error, and consequently, 94% of the recorded intensities originated from incandescence of soot particles. Signal trapping by soot, window fouling and laser energy fluctuations can be seen as attenuations, rather than contaminations, of the LII intensity. Although their effects must be accounted for if quantitative data is required, they need not be accurately assessed for qualitative observations as long as they are not ignored altogether. In the present study laser energy fluctuations were found to affect the LII signal intensity by less than 3%, window fouling resulted in less than 20% attenuation, and LII signal trapping by soot was not quantified but was expected to be moderated by the use of the low-sooting fuel.

#### 4. RESULTS AND DISCUSSION

Figure 3 shows LII intensity profiles for in-cylinder pressures of 6 and 9 MPa, and a range of injection pressures. Similar results were obtained for 7 and 8 MPa in-cylinder pressures. Figure 3 also shows the flame luminosity durations for an in-cylinder pressure of 6 MPa. In all instances the first appearance of LII signal seems to occur slightly earlier for the higher injection pressure cases (140 and 160 MPa). It is interesting to consider that higher injection pressures result in increased injection rates, and therefore at any given time larger proportions of fuel will be undergoing pyrolysis than for lower injection pressures. Consequently, it would seem reasonable to expect soot formation to initiate earlier for the higher injection pressure cases. Following the rise in LII intensity observed in Figure 3, maximums are reached at the end of injections, with values that are dependent on fuel pressure.

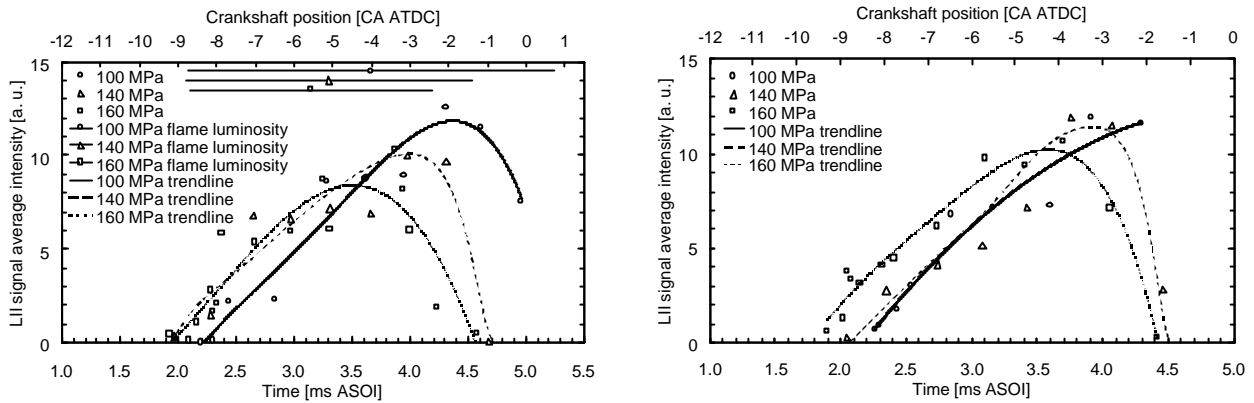


Fig. 3. LII signal intensity profiles for in-cylinder pressures of 6 MPa (left) and 9 MPa (right) at non-fired TDC and a range of injection pressures (100, 140 and 160 MPa at non-fired TDC). Each data point represents the average intensity of at least 27 images. Times are relative to the start of the injection pulse. The durations of the flame luminosity, shown for the 6 MPa in-cylinder pressure plot, were obtained by CCD camera (1 ms exposure).

At the highest injection pressure the lowest peaks in LII signal intensity for all in-cylinder pressures were observed. This can be explained by the fact that higher injection pressures promote the production of smaller fuel droplets (Figure 4) which should, in turn, result in the formation of smaller soot particles that should be more rapidly oxidised. Higher injection pressures also result in longer spray penetration lengths and higher liquid core propagation velocities. Consequently, the transfer of momentum from the liquid spray to the gas phase should be enhanced, improving the mixing of the two phases. Since a better mixing quality corresponds to an increase in the local oxygen content, it is expected that oxidation of soot should be improved. The effects of momentum transfer are expected to be particularly important in the present study due to the quiescent nature of the in-cylinder charge prior to injection (i.e. non-swirl flow). It can also be seen from Figure 3 that flames lasted longer for lower injection pressures. This allowed more time for oxidation at the flame sheath. Since lower fuel pressures are known to result in higher particulate emissions (Bruneaux *et al.*, 1999), it can be concluded that the extended flame duration is not sufficient to oxidise the excess soot production.

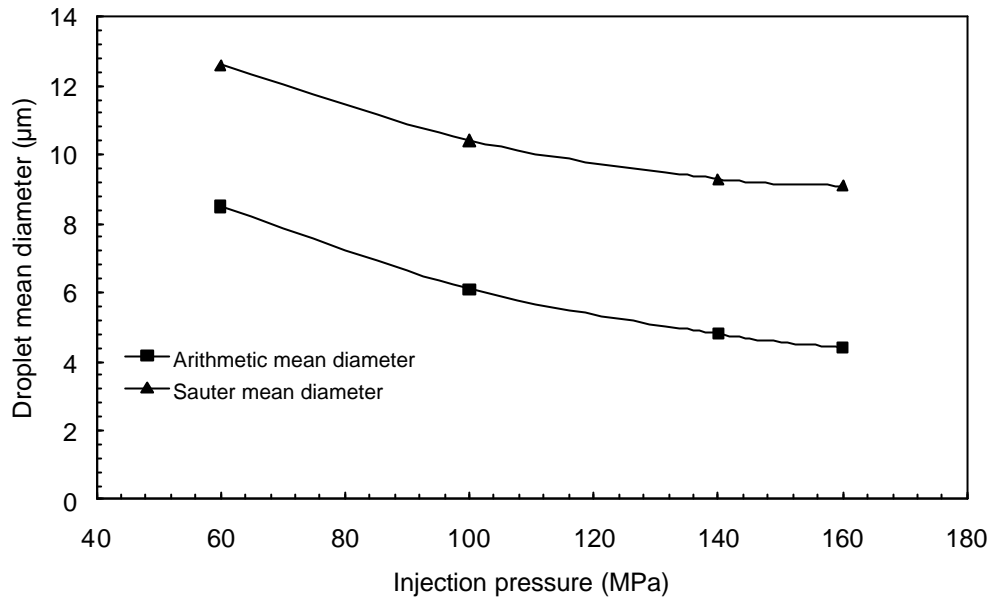
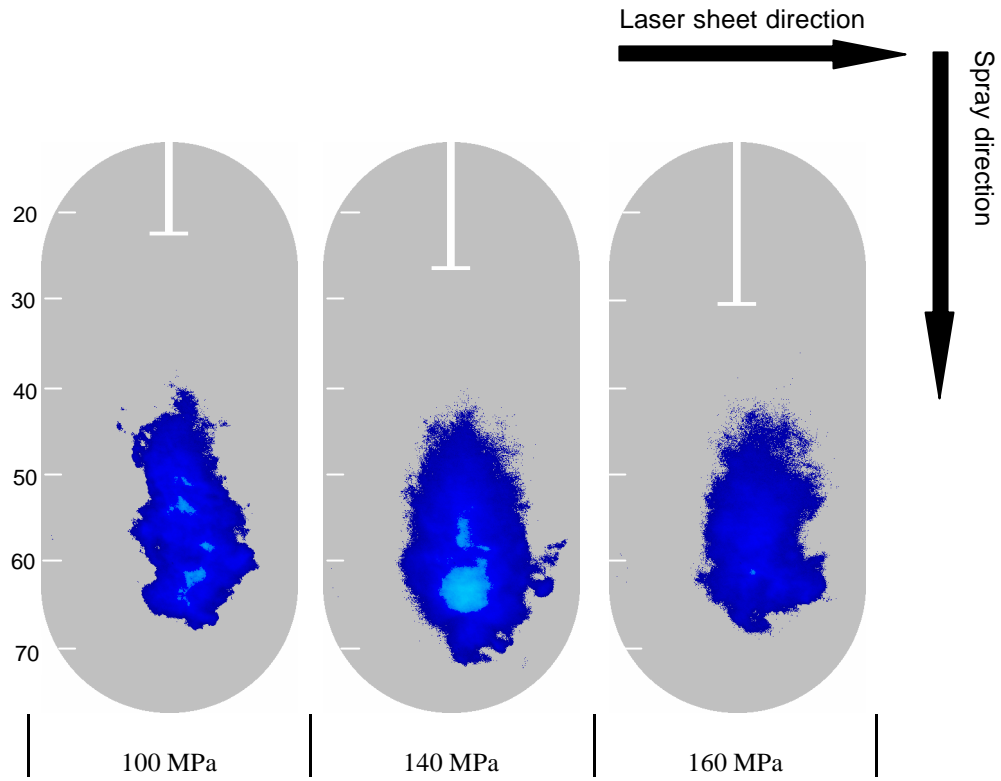


Fig. 4. PDA measurement of the injection pressure effect on droplet mean diameter at 45 mm from the nozzle on the spray axis. Consistent with the trends reported by Araneo (2002) and Koo (1990).

From the analysis of the LII intensity profiles it appeared that the amount of soot produced during combustion was not noticeably affected by a change in in-cylinder pressure. An example of ensemble averaged images showing the influence of injection pressure on early soot formation is presented in Figure 5, for an in-cylinder pressure of 7 MPa. Although the injection pressure has an apparent effect on liquid spray penetration length, the location of the first soot particles detected downstream of the tip of the spray remains almost constant. In Figure 5 the distance from the nozzle to the first soot particles is about 40 mm, and an increase in fuel pressure from 100 MPa to 160 MPa induces a shift of less than 3 mm.





*Fig. 5. Ensemble averaged images showing the effect of injection pressure on initial soot formation sites. Images were recorded between 2.1 and 2.3 ms after start of injection (ASOI), for an ICP of 7 MPa at non-fired TDC. Contrast was enhanced for clarity, white lines show liquid fuel penetration measured by simultaneous LIS, scales indicate distances from the nozzle in millimetres.*

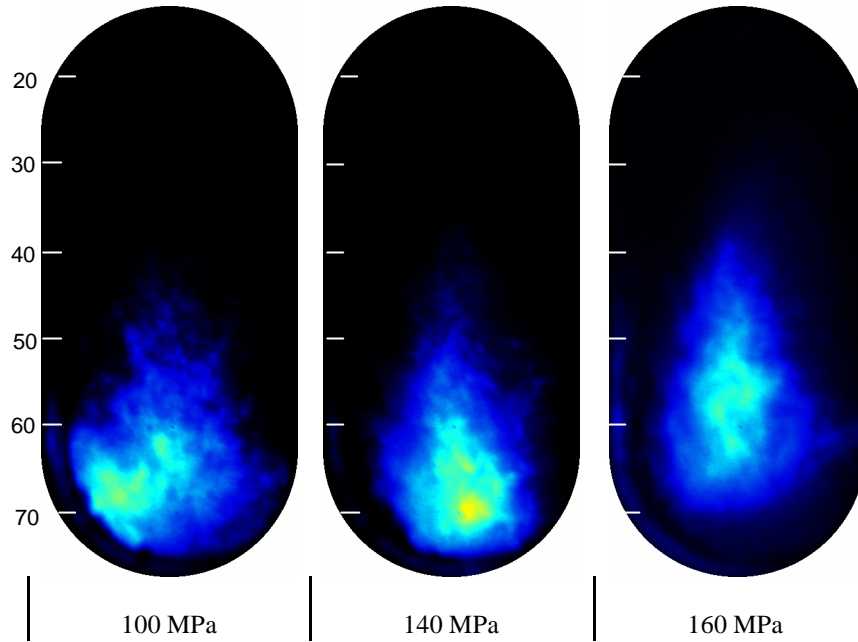


Fig. 6. Ensemble averaged images showing the influence of injection pressure on late soot concentration zones. Images were recorded between 3.5 and 3.6 ms ASOI, for an ICP of 7 MPa at non-fired TDC. Scales indicate distances from the nozzle in millimetres.

Figure 6 illustrates the effect of fuel pressure on late soot concentration. While the lowest injection pressures appear to result in similar soot regions being formed, the LII image is noticeably different for an injection pressure of 160 MPa.

The most striking difference is in the location of the soot region being approximately 10 mm closer to the nozzle orifice. This could be explained by the enhanced vaporisation observed for higher injection pressures (Bruneaux *et al.*, 1999), resulting in faster pyrolysis of the fuel. It is speculated that the formation of soot closer to the nozzle should be beneficial since interactions with the cylinder wall would be reduced. It is also apparent from Figure 6 that the LII signal has a more homogeneous and less intense appearance for the highest injection pressure, suggesting that the soot mass is more uniformly spread within the flame.

While Figures 5 and 6 provide information on the average location of soot and liquid fuel for a large number of cycles, individual LII images can give additional evidence on the structure of soot regions within the flame. In Figure 7, instantaneous images obtained for early (2.2 ms ASOI) and late (3.9 ms ASOI) soot formation are presented. Simultaneous LIS measurement of liquid fuel is shown for the image recorded at 2.2 ms ASOI. As the injection ended at 3.6 ms, no liquid fuel was observed at 3.9 ms. The occurrence of liquid fuel slugs, previously and clustered distribution of dense soot regions are apparent in Figure 7. It is expected that such detachments of groups of droplets should favour soot agglomeration and be strongly detrimental to soot oxidation because of the associated local depletion of oxygen.

For the LII sequences presented thus far (Figure 3), the average time interval between two consecutive data sets was 0.33 ms (1 CA). It was observed that the original appearance of soot is a rapid process and therefore some details may not be apparent at such resolution. In order to obtain a finer series of LII images, the laser system software was automated to record a complete sequence with a data set interval of 50  $\mu$ s (0.15 CA). The resulting sequence comprises 55 images, each image being itself the ensemble average of a 30-image data set. The engine was kept at stable in-cylinder conditions for the whole duration of the recording. The results from this high-resolution sequence are presented in Figure 8, along with results obtained from the spray and combustion measurement techniques.

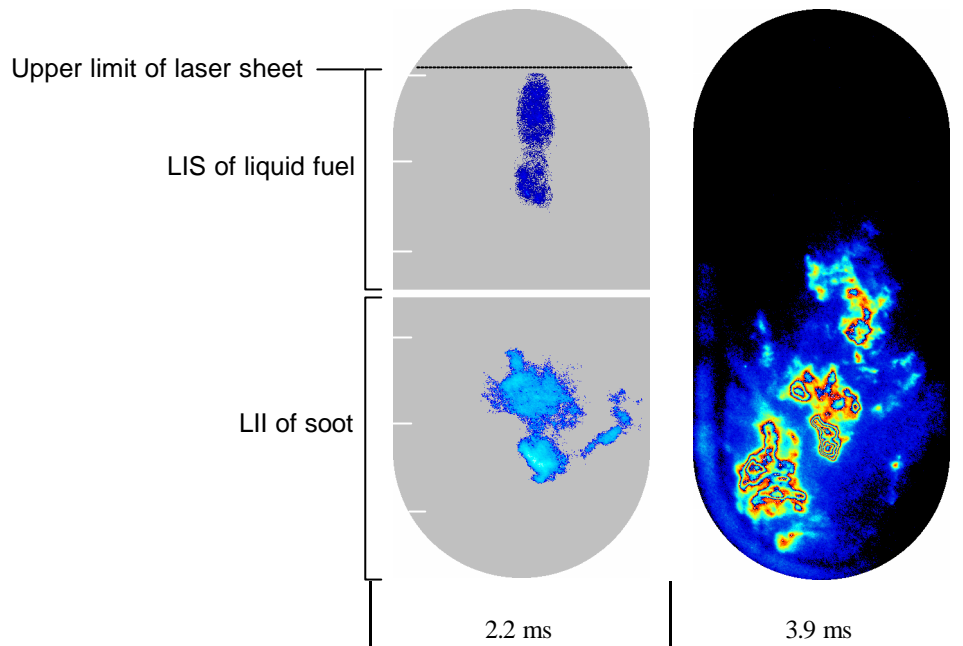


Fig. 7. Examples of liquid and soot clusters for early and late soot formation. 160 MPa injection pressure, 6.0 MPa ICP at TDC, times are relative to start of injection pulse. Contrast of images recorded at 2.2 ms showing simultaneous LIS (upper half) and LII (lower half) was enhanced for clarity.

A wide spray cone angle was also found at the very beginning of the injections, progressively reducing to a narrower mean spray full cone angle of  $10^\circ$  (Figure 8). The occurrence of wide spray cone angles was linked to oscillations of the sprays when the injector's needle was at a short distance from the nozzle orifice.

It was observed that the leading edge of the vapour phase penetrated at a similar rate to the liquid core until the liquid core had reached its ultimate length. After this time the vapour phase penetrated deeper into the chamber due to earlier liquid/air momentum transfer. The vapour penetration profiles were seen to depend on both injection pressure and in-cylinder density. It is suggested that the mechanism for the vapour transport is the gas motion induced by the liquid phase transferring momentum from the droplets to the gas phase. Increased penetration of the vapour was observed at higher injection pressures and lower gas densities, i.e. when the liquid phase had a higher momentum.

Autoignition was found to occur simultaneously at multiple sites within the vapour phase, downstream of the liquid core, which merged and spread quickly through the vapour region. For all the conditions tested, the ignition sites were observed to propagate strictly downstream for the duration of the injection. Only after the injection had stopped, were flames observed to propagate towards the nozzle.

Comparing the LII signal in Figure 8 with the previous LII profiles (Figure 3), one can see that a finer temporal resolution produced a clearer representation of the phases of soot production. The LII signal intensity profile presented in Figure 8 shows that three stages of soot production took place. The first stage is a rapid rise in LII signal that lasted for approximately 0.4 ms, corresponding to elevated soot production rates and low oxidation. An increase in flame luminosity was detected shortly after the first appearance of the LII signal. The diffusion flame, however, was established between 0.2 to 0.3 ms after the autoignition time as observed from autoignition high-speed videos. This leads to establishment of the diffusion flame at a time between 2.3 and 2.4 ms in Figure 8. Then the second stage in soot formation can be distinguished. At this stage higher soot oxidation rates and significantly more fluctuations in soot production are found. This slower soot production phase can be explained by the formation of soot from the ongoing injection, and the concurrent oxidation at the diffusion flame sheath. The third and final phase of soot formation is linked with the end of injection. It is recognised as a sudden decline in soot mass concentrations. While little soot is formed, the oxidation rates at the flame sheath are still high, resulting in a rapid fall in soot concentration. The suggestion made by Flynn *et al.* (1999) that the end of production of soot precursors coincides with the end of injection is corroborated by the results presented here.

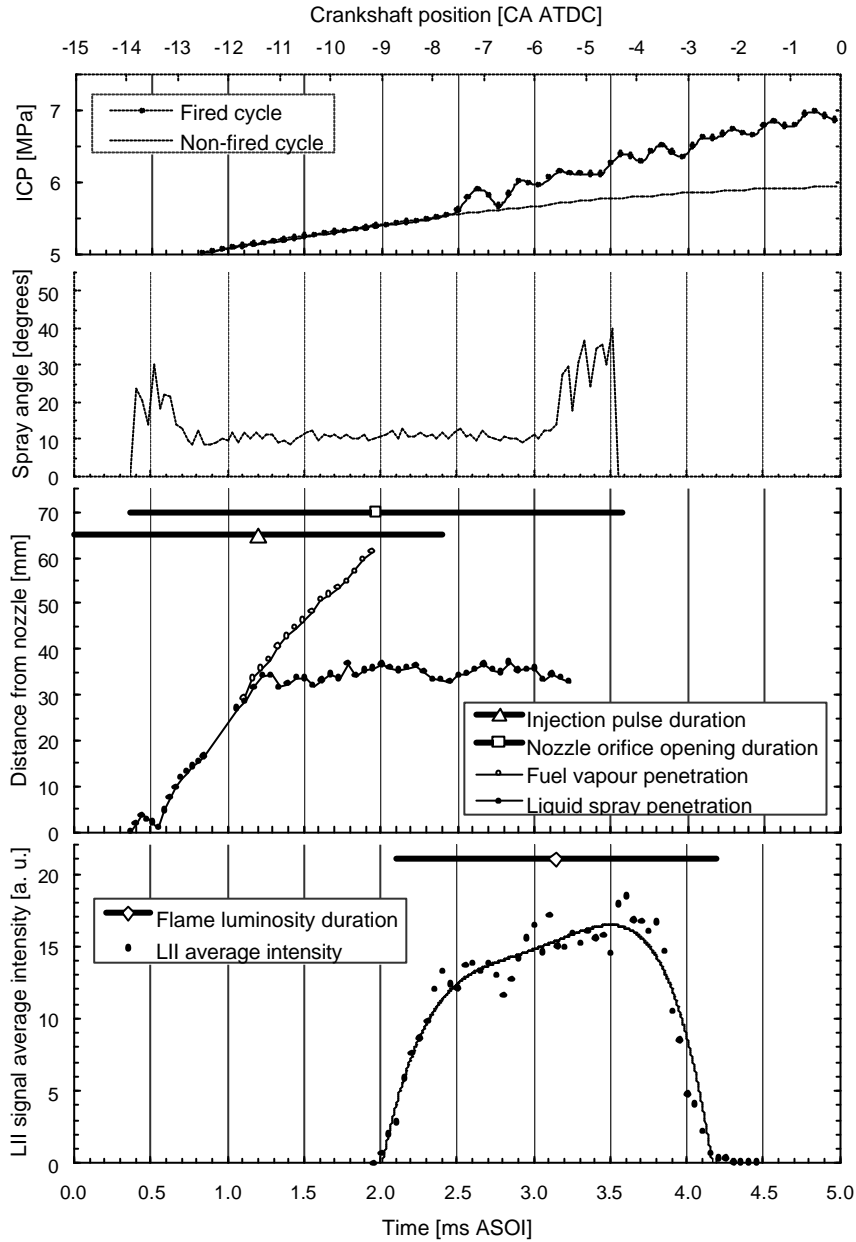


Fig. 8. From top to bottom: in-cylinder pressure traces, spray dispersion full cone angle, fuel liquid and vapour penetrations and injection pulse width, LII of soot with flame luminosity duration. 160 MPa injection pressure, 0.2 mm VCO nozzle. Times are relative to start of injection pulse.

## 5. SUMMARY

Investigations of spray formation, autoignition and soot production performed on an optical diesel engine were presented. Clustered distributions of soot were observed, similar to previously reported images although conflicting with the common assumption that soot is found evenly across the flame. It has been suggested that slugs of fuel detaching from the bulk of the liquid spray favoured soot agglomeration and inhibited soot oxidation due to the associated local depletion of oxygen. The highest injection pressure tested (160 MPa) exhibited lower soot production and more homogeneous soot mass distribution within the flames, for all in-cylinder pressures cases. These effects were related to smaller fuel droplets and better mixing quality, leading to smaller soot particles and improved oxidation,

respectively. Soot particles were detected closer to the liquid spray tip at higher injection pressures. This has been related to enhanced vaporisation of the liquid fuel. It is speculated that formation of soot closer to the nozzle should be beneficial since interactions with the cylinder wall would be reduced. Although the diffusion flames produced with lower injection pressure lasted longer, it appeared that the extended oxidation time was not sufficient to oxidise the excess production of soot.

The recording of a LII sequence at high temporal resolution showed that three distinct phases in soot formation could be observed. High soot production rates were observed from the ignition time until the establishment of diffusion flame. Moderate soot formation rates were observed from the start of diffusion flame until the end of injection. High soot oxidation rates were seen from the end of injection.

## ACKNOWLEDGMENTS

The authors wish to thank David Kennaird, Julien Lacoste and John Evans for their contribution to the collection and analysis of the data. They also wish to acknowledge the financial and technical supports provided by Ricardo Consulting Engineers and the EPSRC (grants GR/R08094/01 and GR/R54774/01).

## REFERENCES

- Araneo, L. and Coghe, A. (2002) "Effect of Injection Conditions on Penetration and Drop Size of HCCI Diesel Sprays", THIESEL 2002, Conference on Thermo- and Fluid Dynamic Processes in Diesel Engines, 173-180.
- Bruneaux, G., Verhoeven, D. and Baritaud, T. (1999). "High Pressure Diesel Spray and Combustion Visualization in a Transparent Model Diesel Engine", SAE report 1999-01-3648.
- Crua, C. (2002). "Combustion Processes in a Diesel Engine", PhD Thesis, University of Brighton (UK).
- Flynn, P.F., Durett, R.P., Hunter, G.L., Zur Loye, A.O., Akinyemi, O.C., Dec, J.E. and Westbrook, C.K. (1999). "Diesel Combustion: An Integrated View Combining Laser Diagnostics, Chemical Kinetics, And Empirical Validation", SAE report 1999-01-0509.
- Kennaird, D.A., Crua, C., Heikal, M., Morgan, R., Bar, F. and Sapsford, S. (2000). "A New High-Pressure Diesel Spray Research Facility", Computational and Experimental Methods in Reciprocating Engines, I.Mech.E. Conf. trans., London (UK) 1-2 November 2000.
- Koo, J. Y. and Martin, J. K. (1990). "Droplet Sizes and Velocities in a Transient Diesel Fuel Spray", SAE Paper 900397.
- Morgan, R., Wray, J., Kennaird, D.A., Crua, C. and Heikal, M. (2001). "The Influence of Injector Parameters on the Formation and Break-Up of a Diesel Spray", SAE Transactions – Journal of Engines 110(3) 389-399; SAE report 2001-01-0529.
- Ni, T., Pinson, J.A., Gupta, S. and Santoro, R.J. (1995) "Two-Dimensional Imaging of Soot Volume Fraction by the Use of Laser-Induced Incandescence", Applied Optics, 34(30), pp. 7083-7091.
- Roth, P. and Filippov, A.V. (1996) J Aerosol Sci., 27(1), pp. 95-104.
- Schraml, S., Will, S. and Leipertz, A. (1999) "Simultaneous Soot Mass Concentration and Primary Particle Size Measurements in the Exhaust Gas of Diesel Engines Based on Laser-Induced Incandescence", 32<sup>nd</sup> ISATA, Vienna (Austria) 14-18 June 1999.
- Tait, N.P. and Greenhalgh, D.A. (1993) "PLIF imaging of fuel fraction in practical devices and LII imaging of soot", Berichte der Bunsengesellschaft fuer Physikalische Chemie, 97 (12), pp. 1619-1625.
- Wainner, R. T. (1999) "An analytical and quantitative analysis of the laser-induced incandescence of soot" PhD Thesis, Georgia Institute of Technology (USA).
- Zhao, H. and Ladommatos N. (1998) "Optical Diagnostics for Soot and Temperature Measurement in Diesel Engines" Prog. Energy Combust Sci., 24, pp. 221-255.